不同阶外激励下压电纤维复合材料悬臂板的内共振特性分析 *

郭翔鹰[1,2†]　段梦烨[1,2]

（1.北京工业大学 材料与制造学部，北京 100124）（2.非线性振动与机械结构强度北京市重点实验室，北京 100124）

摘要　本文研究了不同阶横向激励作用下压电纤维复合材料（MFC）悬臂板的非线性动力学特性.基于Reddy一阶剪切板理论，引入 von Kármán 几何非线性理论，利用 Hamilton 原理建立了结构的非线性动力学控制方程.讨论在不同结构尺寸下的前三阶固有频率，利用 Galerkin 方法将系统离散为三自由度的非线性常微分方程.考虑主参数共振-1:3:5 内共振，分析不同阶外激励作用下压电纤维复合悬臂板的非线性振动响应.数值模拟结果表明，复合材料板几何尺寸增大时结构的固有频率降低.此外，不同阶的横向激励幅值对结构的非线性振动影响很大，为实际工程应用提供理论支持.

关键词　压电纤维复合材料，　非线性，　稳定性分析，　内共振

DOI：10.6052/1672-6553-2020-103

引言

压电纤维复合材料[1-3]（Macro Fiber Composite）是近年来兴起的一种新型压电复合材料（如图1），由 NASA 发明随后由 Smart Material 公司[4]生产进入了商业产品化.作为航空工业界和学术界的研究热点，这种材料已广泛应用于智能结构和设备[5-7].压电纤维复合材料主要由压电纤维，电极和聚合物基质组成，包括MFC-d31和MFC-d33两种[8].

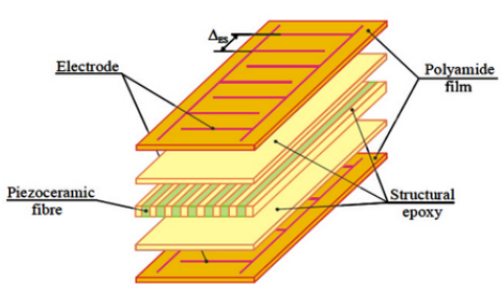

图1　MFC结构组成

Fig.1　MFC configuration

国内外众多力学和材料等相关领域学者们对压电纤维复合材料进行了研究.Williams 等[9]研究了压电纤维复合材料的非线性拉伸和剪切性能.Xia 等[10]基于高阶剪切变形板理论分析了在热环境下，表面粘结压电纤维增强复合材料驱动器的功能梯度材料板的非线性动态响应.Shen 等[11]基于高阶剪切板理论，考虑压电材料的温度依赖性和初始的几何缺陷，研究了压电层合板的热屈曲行为.Padoin 等[12]在复合材料层合板中贴放压电纤维复合材料，并通过改变复合材料层合板的铺设方式讨论压电纤维复合材料的减振抑制作用.Guo 等[13]应用 Reddy 三阶剪切理论分析压电纤维复合材料中厚度壳的动力学特性，结果表明压电纤维复合材料具有良好的抑制振动作用.Jiang 等[14]分析了石墨烯及压电纤维复合材料板的非线性动力学特性.Panda 等[15]通过主动约束层理论研究了在几何大变形下功能梯度压电纤维复合材料层压板的非线性动力学特性.Xie 等[16]基于高阶剪切变形理论，在反平面剪切和平面内电载荷作用下，对具有任意形状夹杂的压电纤维复合材料进行二维电弹性分析.

基于上述文献综述表明，压电纤维复合材料对振动抑制以及结构振动响应都有一定的影响.本文主要研究不同阶激励作用下压电纤维复合材料板结构的非线性动态特性响应，分析压电纤维复合材料悬臂板主参数共振-1:3:5 内共振情况下的非线

2020-09-22 收到 1 稿，2020-10-22 收到修改稿.

* 国家自然科学基金资助项目（11572006，11772010）

† 通讯作者 E-mail：eagle2008guo@yeah.net

性动力学响应.

1 运动方程

以无人机机翼作为工程背景,将机翼简化为压电纤维复合材料的悬臂板结构,选择 d-31 类型的压电纤维复合材料,建立如图 2 所示的力学模型,直角坐标 oxy 位于压电纤维复合材料板的中性面内,z 轴向下,设板内任一点沿 x、y 和 z 方向的位移分别为 u、v 和 w,并在该板上施加横向激励.悬臂板模型的长为 a,宽为 b,厚度为 h.根据 Reddy 一阶剪切理论,忽略面内位移,压电纤维复合材料悬臂板的位移场在笛卡尔坐标系中表示如下

$$u(x,y,z,t)=u_0(x,y,t)-z\phi_x \tag{1a}$$

$$v(x,y,z,t)=v_0(x,y,t)-z\phi_y \tag{1b}$$

$$w(x,y,z,t)=w_0(x,y,t) \tag{1c}$$

式中,u,v,w 为沿着 x、y、z 三个坐标轴方向的位移;u_0,v_0 为薄板中面沿着 x、y 方向的位移;$\phi_x=-\kappa\dfrac{\partial w_0}{\partial x}$,$\phi_y=-\kappa\dfrac{\partial w_0}{\partial y}$ 为转角,κ 为剪切修正因子.

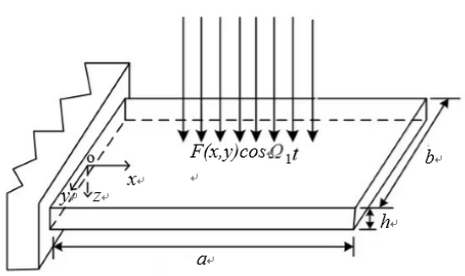

图 2 压电纤维复合材料悬臂板的动力学模型

Fig.2 The macro fibre composite plate model

引入 Von Kármán 几何非线性,得到应变和位移关系的非线性表达式如下

$$\varepsilon_{xx}=\frac{\partial u}{\partial x}+\frac{1}{2}\left(\frac{\partial w_0}{\partial x}\right)^2=\frac{\partial u_0}{\partial x}-z\kappa\frac{\partial^2 w_0}{\partial x^2}+\frac{1}{2}\left(\frac{\partial w_0}{\partial x}\right)^2 \tag{2a}$$

$$\varepsilon_{yy}=\frac{\partial v}{\partial y}+\frac{1}{2}\left(\frac{\partial w_0}{\partial y}\right)^2=\frac{\partial v_0}{\partial y}-z\kappa\frac{\partial^2 w_0}{\partial y^2}+\frac{1}{2}\left(\frac{\partial w_0}{\partial y}\right)^2 \tag{2b}$$

$$\gamma_{xy}=\frac{\partial u}{\partial y}+\frac{\partial v}{\partial x}+\frac{\partial^2 w}{\partial x\partial y}=\frac{\partial u_0}{\partial y}+\frac{\partial v_0}{\partial x}+\frac{\partial^2 w_0}{\partial x\partial y}-2z\kappa\left(\frac{\partial^2 w_0}{\partial x^2}+\frac{\partial^2 w_0}{\partial y^2}\right) \tag{2c}$$

$$\gamma_{yz}=\frac{\partial v_0}{\partial y}-\kappa\frac{\partial w_0}{\partial y},\gamma_{xz}=\frac{\partial u_0}{\partial x}-\kappa\frac{\partial w_0}{\partial x},\varepsilon_{zz}=0 \tag{2d}$$

压电纤维复合材料的本构关系如下

$$\begin{Bmatrix}\sigma_{xx}\\ \sigma_{yy}\\ \tau_{xy}\end{Bmatrix}=\begin{pmatrix}Q_{11}&Q_{12}&0\\ Q_{21}&Q_{22}&0\\ 0&0&Q_{66}\end{pmatrix}\left(\begin{Bmatrix}\varepsilon_{xx}\\ \varepsilon_{yy}\\ \gamma_{xy}\end{Bmatrix}-\begin{Bmatrix}d_{31}\\ d_{32}\\ 0\end{Bmatrix}E_3\right) \tag{3}$$

其中,d_{31},d_{32} 为压电纤维的压电应变系数,E_3 为压电纤维的电场强度,$d_{3i}\cdot E_3(i=1,2)$ 为由电场产生的应变.压电纤维复合材料采用正交铺设的方式.其中,$Q_{11}=Q_{22}=\dfrac{E}{1-\mu^2}$,$Q_{12}=Q_{21}=\dfrac{\mu E}{1-\mu^2}$,$Q_{66}=\dfrac{E}{2(1-\mu^2)}$,$E$ 为杨氏模量,μ 为材料的泊松比.将式(1)~式(3)代入 Hamilton 原理,得到广义位移形式下表示的系统非线性动力学方程

$$\begin{aligned}&a_{11}\frac{\partial^2 u_0}{\partial x^2}+a_{12}\frac{\partial w_0}{\partial x}\frac{\partial^2 w_0}{\partial x^2}+a_{13}\frac{\partial^2 v_0}{\partial x\partial y}+\\&\quad a_{14}\frac{\partial w_0}{\partial y}\frac{\partial^2 w_0}{\partial x\partial y}+a_{15}\frac{\partial^2 u_0}{\partial y^2}+a_{16}\frac{\partial w_0}{\partial x}\frac{\partial^2 w_0}{\partial y^2}\\&=a_{17}\frac{\partial^2 u_0}{\partial t^2}+a_{18}\frac{\partial^2 w_0}{\partial t^2\partial x}\end{aligned} \tag{4a}$$

$$\begin{aligned}&b_{11}\frac{\partial^2 v_0}{\partial y^2}+b_{12}\frac{\partial w_0}{\partial y}\frac{\partial^2 w_0}{\partial y^2}+b_{13}\frac{\partial^2 u_0}{\partial x\partial y}+\\&\quad b_{14}\frac{\partial w_0}{\partial x}\frac{\partial^2 w_0}{\partial x\partial y}+b_{15}\frac{\partial^2 v_0}{\partial x^2}+b_{16}\frac{\partial w_0}{\partial y}\frac{\partial^2 w_0}{\partial x^2}\\&=b_{17}\frac{\partial^2 v_0}{\partial t^2}+b_{18}\frac{\partial^2 w_0}{\partial t^2\partial y}\end{aligned} \tag{4b}$$

$$\begin{aligned}&c_{11}\frac{\partial w_0}{\partial x}\frac{\partial w_0}{\partial y}\frac{\partial^2 w_0}{\partial x\partial y}+c_{12}\frac{\partial w_0}{\partial x}\frac{\partial^2 u_0}{\partial y^2}+\\&\quad c_{13}\frac{\partial u_0}{\partial x}\frac{\partial^2 w_0}{\partial^2 y}+c_{14}\frac{\partial w_0}{\partial x}\frac{\partial^2 u_0}{\partial^2 x}+\\&c_{15}\left(\frac{\partial w_0}{\partial x}\right)^2\frac{\partial^2 w_0}{\partial y^2}+c_{16}\frac{\partial w_0}{\partial y}\frac{\partial^2 u_0}{\partial x\partial y}+c_{17}\frac{\partial w_0}{\partial x}\frac{\partial^2 v_0}{\partial x\partial y}+\\&\quad c_{18}\left(\frac{\partial w_0}{\partial y}\right)^2\frac{\partial^2 w_0}{\partial^2 y}+\\&c_{19}\frac{\partial w_0}{\partial y}\frac{\partial^2 v_0}{\partial^2 y}+c_{20}\frac{\partial v_0}{\partial y}\frac{\partial^2 w_0}{\partial x^2}+c_{21}\frac{\partial w_0}{\partial y}\frac{\partial^2 u_0}{\partial x\partial y}+\\&\quad c_{22}\frac{\partial w_0}{\partial x}\frac{\partial^2 v_0}{\partial x\partial y}+c_{23}\left(\frac{\partial w_0}{\partial y}\right)^2\frac{\partial^2 w_0}{\partial^2 y}+\\&c_{24}\frac{\partial w_0}{\partial y}\frac{\partial^2 v_0}{\partial^2 y}+c_{25}\frac{\partial v_0}{\partial y}\frac{\partial^2 w_0}{\partial x^2}+c_{26}\frac{\partial w_0}{\partial y}\frac{\partial^2 v_0}{\partial x^2}+\\&c_{27}\frac{\partial v_0}{\partial x}\frac{\partial^2 w_0}{\partial x\partial y}+c_{28}\frac{\partial^2 w_0}{\partial^2 x}+c_{29}\frac{\partial^2 w_0}{\partial^2 y}+c_{30}\frac{\partial^4 w_0}{\partial^4 x}+\\&\quad c_{31}\frac{\partial^4 w_0}{\partial x^2\partial y^2}+c_{32}\frac{\partial^4 w_0}{\partial y^4}+F\cos(\Omega_1 t)+c_{33}\dot{w}_0\end{aligned}$$

$$= c_{34}\frac{\partial^2 w_0}{\partial t^2} + c_{35}\frac{\partial^4 u_0}{\partial x^2\partial t^2} + c_{36}\frac{\partial^4 v_0}{\partial y^2\partial t^2} + c_{37}\frac{\partial^4 w_0}{\partial x^2\partial t^2} + c_{38}\frac{\partial^4 w_0}{\partial y^2\partial t^2} \tag{4c}$$

其中,$F\cos(\Omega_1 t)$为横向激励幅值,μ为阻尼系数.悬臂板的边界条件为

$$x = 0: w = 0, \frac{\partial w_0}{\partial x} = \frac{\partial w_0}{\partial y} = 0 \tag{5a}$$

$$x = a: N_{xx} = N_{xy} = M_{xx} = 0 \tag{5b}$$

$$y = 0, b: N_{yy} = N_{xy} = M_{yy} = 0 \tag{5c}$$

2　Galerkin离散

采用Galerkin方法,选取合适的基本函数组合为系统模态函数,将偏微分方程进行三阶离散,得到压电纤维复合材料悬臂板横向振动的常微分形式动力学方程,首先引入如下的无量纲变量

$$\bar{u} = \frac{u_0}{a}, \bar{v} = \frac{v_0}{b}, \bar{w} = \frac{w_0}{h}, \bar{t} = \frac{\pi^2 t}{\sqrt{E}}(ab\rho)^{\frac{1}{2}}, \bar{x} = \frac{a}{x}$$

$$\bar{A}_{ij} = \frac{(ab)^{\frac{1}{2}}A_{ij}}{Eh^2}, \bar{D}_{ij} = \frac{(ab)^{\frac{1}{2}}D_{ij}}{Eh^4}, \bar{y} = \frac{b}{y},$$

$$\bar{I}_i = \frac{I_i}{\rho(\sqrt{ab})^{i+1}}, \bar{F} = \frac{(ab)^{\frac{7}{2}}}{Eh^7}F,$$

$$\bar{N}_{e1} = \frac{(ab)^{\frac{7}{2}}}{Eh^7}N_{e1}, \bar{N}_{e2} = \frac{(ab)^{\frac{7}{2}}}{Eh^7}N_{e2} \tag{6}$$

根据悬臂板边界条件,选取如下的模态函数对系统的动力学方程进行Galerkin三阶离散

$$u_0(x,y,t) = u_1\sin(\frac{\pi x}{2a})\cos(\frac{\pi y}{b}) + u_2\sin(\frac{\pi x}{2a})\cos(\frac{3\pi y}{b}) + u_3\sin(\frac{3\pi x}{2a})\cos(\frac{3\pi y}{b}) \tag{7a}$$

$$v_0(x,y,t) = v_1\sin(\frac{\pi x}{2a})\cos(\frac{\pi y}{b}) + v_2\sin(\frac{\pi x}{2a})\cos(\frac{3\pi y}{b}) + v_3\sin(\frac{3\pi x}{2a})\cos(\frac{3\pi y}{b}) \tag{7b}$$

$$w(x,y,t) = w_1(t)X_1Y_1 + w_2(t)X_1Y_2 + w_3(t)X_2Y_1 \tag{7c}$$

式中$w_1w_2w_3$分别表示系统第一阶、第二阶和第三阶模态的振动幅值,X_i和Y_i的表达式为

$$X_i(x) = \sin\lambda_i x - \sinh\lambda_i x + \alpha_i(\cosh\lambda_i x - \cos\lambda_i x) \tag{8a}$$

$$Y_1(y) = 1,\ Y_2(y) = \sqrt{3}\left(1 - \frac{2y}{b}\right) \tag{8b}$$

$$\cos\lambda_i a\cosh\lambda_i a + 1 = 0 \tag{8c}$$

$$\alpha_i = \frac{\sinh\lambda_i a + \sin\lambda_i a}{\cosh\lambda_i a + \cos\lambda_i a} \tag{8d}$$

横向激励和压电参数的离散形式为

$$F = F_1(t)\sin(\frac{\pi x}{2a})\sin(\frac{\pi y}{b}) + F_2(t)\sin(\frac{\pi x}{2a})\sin(\frac{3\pi y}{b}) + F_3(t)\sin(\frac{3\pi x}{2a})\sin(\frac{3\pi y}{b}) \tag{9a}$$

$$N_{e1} = N_{e11}\sin(\frac{\pi x}{2a})\cos(\frac{\pi y}{b}) + N_{e12}\sin(\frac{\pi x}{2a})\cos(\frac{3\pi y}{b}) + N_{e13}\sin(\frac{3\pi x}{2a})\cos(\frac{3\pi y}{b}) \tag{9b}$$

$$N_{e2} = N_{e21}\sin(\frac{\pi x}{2a})\cos(\frac{\pi y}{b}) + N_{e22}\sin(\frac{\pi x}{2a})\cos(\frac{3\pi y}{b}) + N_{e23}\sin(\frac{3\pi x}{2a})\cos(\frac{3\pi y}{b}) \tag{9c}$$

其中,N_{e1},N_{e2}分别表示的是由压电产生的力,将以上模态代入到无量纲后的动力学方程中,得到悬臂板三阶离散后的常微分控制方程,如下

$$\ddot{w}_1 + \mu_1\dot{w}_1 + \omega_1^2 w_1 + k_{11}w_1^3 + k_{12}w_2^3 + k_{13}w_3^3 + k_{14}w_1w_2^2 + k_{15}w_1w_3^2 + k_{16}w_2w_1^2 + k_{17}w_2w_3^2 + k_{18}w_3w_1^2 + k_{19}w_3w_2^2 + k_{110}w_1w_2w_3 + p_1\cos(\Omega_2 t)w_1 = k_{111}F_1\cos\Omega_1 t \tag{10a}$$

$$\ddot{w}_2 + \mu_2\dot{w}_2 + \omega_2^2 w_2 + k_{21}w_1^3 + k_{22}w_2^3 + k_{23}w_3^3 + k_{24}w_1w_2^2 + k_{25}w_1w_3^2 + k_{26}w_2w_1^2 + k_{27}w_2w_3^2 + k_{28}w_3w_1^2 + k_{29}w_3w_2^2 + k_{210}w_1w_2w_3 + p_2\cos(\Omega_2 t)w_2 = k_{211}F_2\cos\Omega_1 t \tag{10b}$$

$$\ddot{w}_3 + \mu_3\dot{w}_3 + \omega_3^2 w_3 + k_{31}w_1^3 + k_{32}w_2^3 + k_{33}w_3^3 + k_{34}w_1w_2^2 + k_{35}w_1w_3^2 + k_{36}w_2w_1^2 + k_{37}w_2w_3^2 + k_{38}w_3w_1^2 + k_{39}w_3w_2^2 + k_{310}w_1w_2w_3 + p_3\cos(\Omega_2 t)w_3 = k_{311}F_3\cos\Omega_1 t \tag{10c}$$

其中,ω_1,ω_2和ω_3分别为结构的前三阶固有频率,p_i(i=1,2,3)为压电系数.

3　固有频率分析

根据压电纤维复合材料悬臂板的动力学模型,利用ANSYS有限元结构分析软件建立了有限元模型,表1给出了压电纤维复合材料悬臂板的几何参数,根据几何参数,解得前三阶的固有频率如表2

及模态振型如图3所示.

表1 压电纤维复合材料悬臂板的几何参数

Table 1 Geometric parameters of the piezoelectric fiber composite cantilever plate

Material properties	MFC
Length(m)	0.085
Width(m)	0.050
Height(m)	0.0003
Young′s modulus (GPa)	210
Density (kg·m^{-3})	5440
Poisson′s ratio	0.16
Piezoelectric gauge factor (PC/N)	$d_{31}=-185\times10^{-12}$ $d_{32}=400\times10^{-12}$

由有限元模态分析结果得出,压电纤维复合材料悬臂板结构前三阶模态的模式为:第一阶弯曲振动,第二阶扭转振动,第三阶弯曲振动.为进一步分析压电纤维复合材料悬臂板几何尺寸对固有频率的影响,固定宽度为0.05m,改变悬臂板的长度,得到不同长宽比下压电悬臂板的前三阶固有频率.如表3及图4所示的为不同长宽比下结构的固有频率值,随着长宽比的增加,前三阶固有频率逐渐降低.

表2 压电纤维复合材料悬臂板的前三阶固有频率

Table 2 The first three natural frequencies

Order	Natural frequency(Hz)
First order frequency	36.46
Second order frequency	123.26
Third order frequency	233.54

4 内共振分析

由于内共振会引起结构动态不稳定甚至失效破坏,所以需要对不同长宽比下系统存在的内共振现象进行分析,根据上述固有频率的分析,在此研究1:3:5内共振关系,采用多尺度法,得到系统极坐标形式的平均方程为

$$\dot{a}_1=-\frac{1}{2}\mu_1 a_1-\frac{1}{8}k_{16}a_1^2a_2\sin(3\beta_2-3\beta_1)+\frac{1}{8}k_{110}a_1a_2a_3\sin(-2\beta_1-3\beta_2+5\beta_3)+\frac{1}{4}p_1a_1-\frac{k_{111}F_1}{2}\sin\beta_1 \tag{11a}$$

$$a_1\dot{\beta}_1=\sigma_1a_1+\frac{1}{4}k_{11}a_1^3+\frac{1}{4}k_{14}a_1a_2^2+\frac{1}{4}k_{15}a_1a_3^2+\frac{1}{8}k_{16}a_1^2a_2\cos(3\beta_2-3\beta_1)+\frac{1}{8}k_{110}a_1a_2a_3\cos(-2\beta_1-3\beta_2+5\beta_3)+\frac{1}{4}p_1a_1+\frac{k_{111}F_1}{2}\cos\beta_1 \tag{11b}$$

$$\dot{a}_2=-\frac{1}{2}\mu_2a_2-\frac{1}{24}k_{21}a_1^3\sin(3\beta_1-3\beta_2)-$$

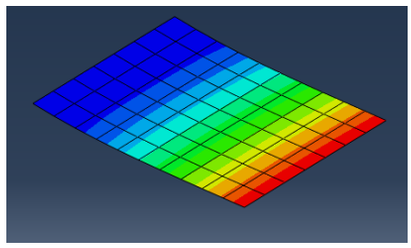

(a)第一阶弯曲模态振动态振动

(a)The first order bending modal vibration

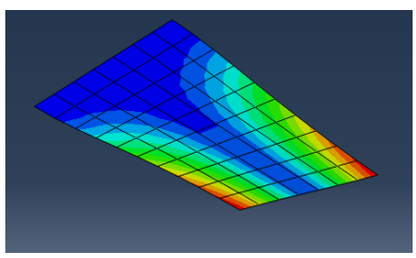

(b)第二阶扭转模态振动

(b)The second order torsinal modal vibration

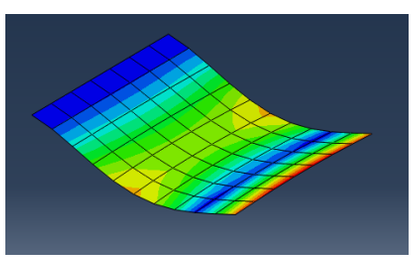

(c)第三阶弯曲模态振动

(c)The third order bending modal vibration

图3 压电纤维复合材料悬臂板前三阶模态振型图

Fig.3 The first three vibration modes of the piezoelectric fiber composite cantilever plate

表3 压电纤维复合材料悬臂板不同长宽比的前三阶固有频率

Table 3 The first three natural frequencies with different aspect ratios

Size(m)	The first order (Hz)	The second order(Hz)	The third order (Hz)
a=0.05	106.6	185.17	635.07
a=0.085	36.714	123.26	233.54
a=0.10	26.24	114.88	161.66
a=0.15	11.74	60.18	71.99
a=0.175	8.46	52.41	62.08
a=0.2	6.46	40.06	53.89

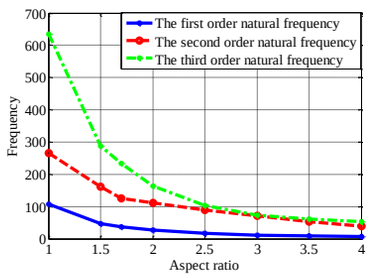

图4　不同长宽比下的压电纤维复合材料悬臂板前三阶固有频率

Fig.4　The first three natural frequencies corresponding to different aspect ratios

$$\frac{1}{24}k_{28}a_1^2a_3\sin(-2\beta_1-3\beta_2+5\beta_3)+\frac{1}{24}k_{210}a_1a_2a_3\sin(\beta_1-6\beta_2+5\beta_3)\tag{11c}$$

$$a_2\dot{\beta}_2=\sigma_2a_2+\frac{1}{24}k_{21}a_1^3\cos(3\beta_1-3\beta_2)+\frac{1}{12}k_{22}a_2^3+\frac{1}{12}k_{26}a_1^2a_2+\frac{1}{12}k_{27}a_2a_3^2-\frac{1}{6}p_2a_2+\frac{1}{24}k_{28}a_1^2a_3\cos(-2\beta_1-3\beta_2+5\beta_3)+\frac{1}{24}k_{210}a_1a_2a_3\cos(\beta_1-6\beta_2-5\beta_3)\tag{11d}$$

$$\dot{a}_3=-\frac{1}{2}\mu_3a_3-\frac{1}{40}k_{36}a_1^2a_2\sin(2\beta_1+3\beta_2-5\beta_3)\tag{11e}$$

$$a_3\dot{\beta}_3=\sigma_3a_3+\frac{1}{40}k_{33}a_3^3+\frac{1}{40}k_{36}a_1^2a_2\cos(2\beta_1+3\beta_2-5\beta_3)+\frac{1}{40}k_{38}a_1^2a_3+\frac{1}{40}k_{39}a_2^2a_3+\frac{1}{20}p_3a_3\tag{11f}$$

通过数值模拟方法分析压电纤维复合材料悬臂板结构的非线性动力学行为,研究压电系数及外激励幅值对结构振动响应的影响.由表1的结构参数,计算无量纲后的系数.其中,$\mu_1=0.32$,$\mu_2=0.32$,$\mu_3=0.32$,$\beta_1=\pi/2$,$\beta_2=\pi/3$,$\beta_3=\pi/4$,$k_{11}=10.2$,$k_{14}=0.66$,$k_{15}=-0.5$,$k_{16}=5.2$,$k_{110}=12.7$,$k_{111}=15.8$,$k_{21}=-39.2$,$k_{22}=6.98$,$k_{26}=4.15$,$k_{27}=11.5$,$k_{28}=1.55$,$k_{210}=5.92$,$k_{33}=-8.1$,$k_{36}=1.55$,$k_{38}=2.35$,$k_{39}=-8.73$,$p_1=1.0$,$p_2=1.0$,$p_3=1.0$,改变外激励幅值,令外激励F_1分别为100,300和500,得到在不同外激励情况下的幅频特性曲线如图5所示,系统呈现硬弹簧特性,并随着外激励的增大,硬弹簧特性增强.另外,压电项对MFC悬臂板的非线性响应有着重要的影响,固定上述的参数值和初始条件,如图6所示的不同压电系数下前三阶的幅频特性曲线,压电系数p_i分别取20,50和80,系统呈现硬弹簧特性,随着压电系数的增大,硬弹簧特性增强.

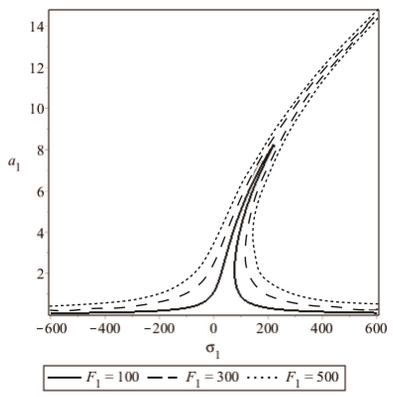

图5　一阶外激励作用下的幅频响应曲线

Fig.5　The amplitude-frequency response curve under external force of the first order (F_1)

5　非线性动态特性响应

为了分析压电纤维复合材料悬臂板的非线性振动特性,通过低频激发高频以及高频激发低频,分析不同尺寸下前三阶外激励对板振动的影响.采用Runge-Kutta法对悬臂板进行数值模拟,借助MATLAB数值模拟绘制分叉图研究外激励对结构前三阶非线性振动响应的影响.

5.1　长度为0.085,宽度为0.05的系统动态响应

当悬臂板的长为0.085,宽为0.05时,分别改变前三阶的外激励幅值,研究振动响应随外激励幅值的变化情况.当幅值F_1从0变化到300的过程中,得到系统一阶外激励的对系统非线性动力学行为的影响,其分叉图如图7所示,从分叉图中分析可得:系统在开始时具有周期性运动,然后在短暂振荡后进入周期性运动.

图8所示为外激励F_2作用下的前三阶分叉图.由图可知系统随着外激励F_2的增加,最开始进行周期运动,当F_2=160时,系统出现分叉,进入混沌运动,当F_2增大到250N时,系统又重新呈现较为稳定的倍周期运动.与第一阶外激励F_1作用下的前三阶分叉图相比发现,不论是F_1还是F_2的作用,第三阶的分叉现象更为明显,且分叉区域较大.

图9为第三阶外激励F_3作用下的前三阶分叉图.由图可知系统随着外激励F_3的增加,最开始进行周期运动,当F_3=100时,系统从周期运动进入混沌运动,从图中看出F_3对第三阶的影响更显著,混

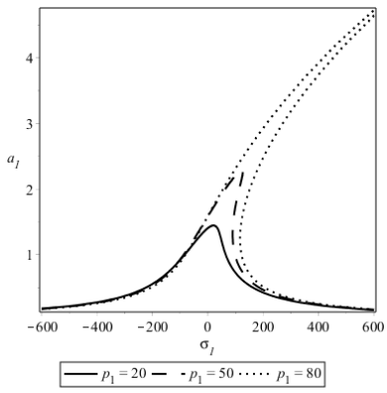

(a)第一阶幅频响应曲线

(a)The first order amplitude response curve

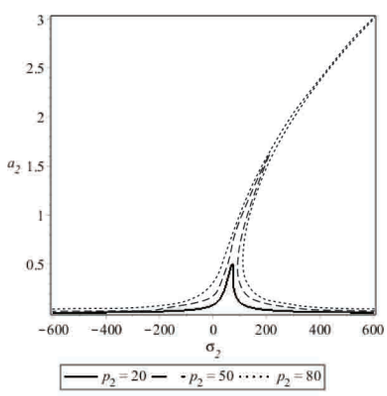

(b)第二阶幅频响应曲线

(b)The second order amplitude response curve

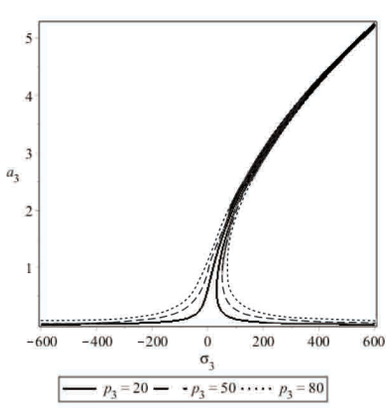

(c)第三阶幅频响应曲线

(c)The third order amplitude response curve

图6 前三阶不同压电系数下的幅频特性曲线

Fig.6 The amplitude-frequency response curves with different piezoelectric coefficients of the first three orders

沌区域更大,第一阶和第二阶的分叉图呈现相同的趋势.由上述分析可知,不同外激励作用下系统都呈现周期混沌运动的现象,通过横向比较不同阶的三个外部激励的分叉图,发现系统的高阶响应中混沌区域增加了,混沌现象更加显著.

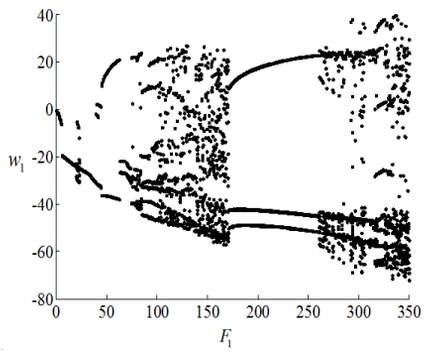

(a)第一阶分叉图

(a)The first-order bifurcation diagram

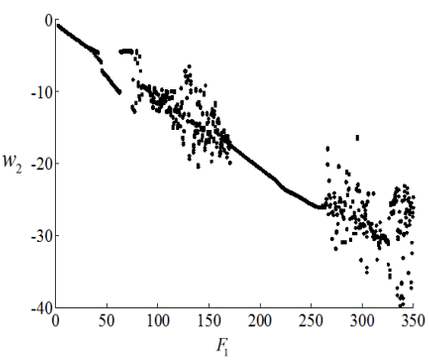

(b)第二阶分叉图

(b)The second-order bifurcation diagram

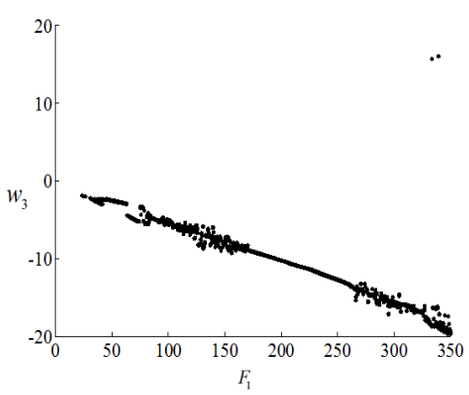

(c)第三阶分叉图

(c)The third-order bifurcation diagram

图7 系统随一阶外激励变化的分叉图

Fig.7 The bifurcation diagrams of the first three modes with respect to excitation amplitude F_1

5.2 长度为0.1,宽度为0.05的系统动态响应

为了进一步分析压电纤维复合材料悬臂板在低频和高频下的响应,改变板的尺寸继续分析板的稳定性,令长度为0.1,宽度为0.05,仅改变悬臂板的尺寸并固定压电纤维复合材料的其他物理参数,再次研究不同阶外激励作用下结构响应的分叉图.

当一阶外部激励变化时(如图10所示),在F_1=

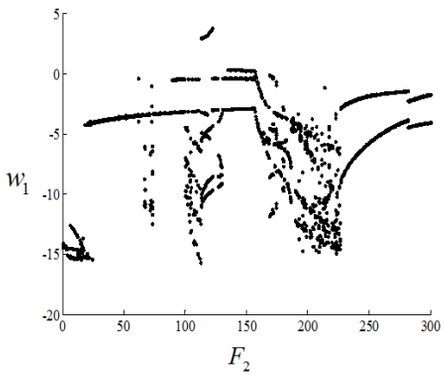

(a)第一阶分叉图

(a)The first-order bifurcation diagram

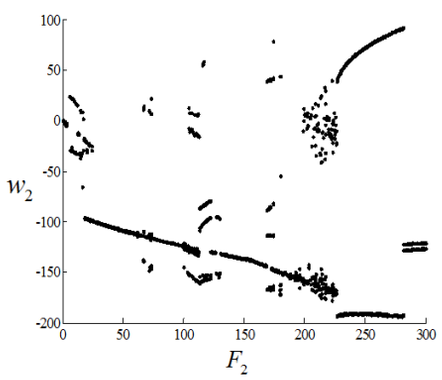

(b)第二阶分叉图

(b)The second-order bifurcation diagram

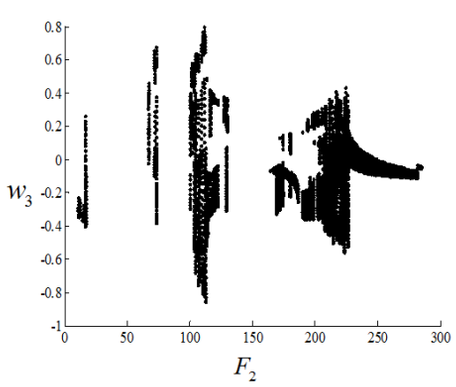

(c)第三阶分叉图

(c)The third-order bifurcation diagram

图 8　系统随二阶外激励变化的分叉图

Fig.8　The bifurcation diagrams of the first three modes with respect to excitation amplitude F_2

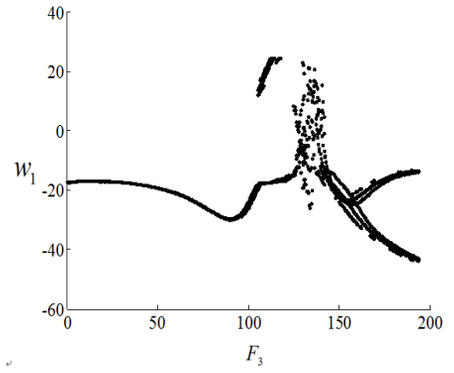

(a)第一阶分叉图

(a)The first-order bifurcation diagram

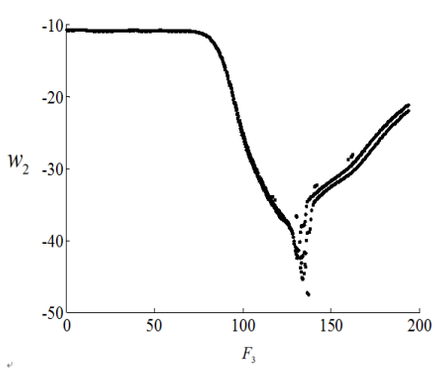

(b)第二阶分叉图

(b)The second-order bifurcation diagram

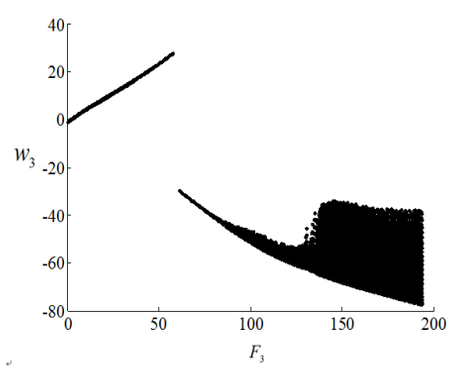

(c)第三阶分叉图

(c)The third-order bifurcation diagram

图 9　系统随三阶外激励变化的分叉图

Fig.9　The bifurcation diagrams of the first three modes with respect to excitation amplitude F_3

250时,系统存在混沌运动,当二阶外部激励变化时(如图 11 所示),在 F_2=210时,系统存在混沌运动,当三阶外部激励变化时(如图 12 所示),在 F_3=280时,系统存在混沌运动.由图 10–图 12 可知,随着悬臂板几何尺寸的增加,系统的稳定性降低.同样,F_1 和 F_2 对高阶响应的影响更大,系统的混沌区域更大,混沌现象更加明显.

6　结论

本文研究了在横向激励作用下,压电纤维复合材料悬臂板的非线性动力学响应.应用Reddy一阶剪切变形理论,von Karman 位移–应变关系和 Hamilton 原理建立系统无量纲偏微分动力学方程,采用 Galerkin 方法对系统进行三阶离散,得到三自

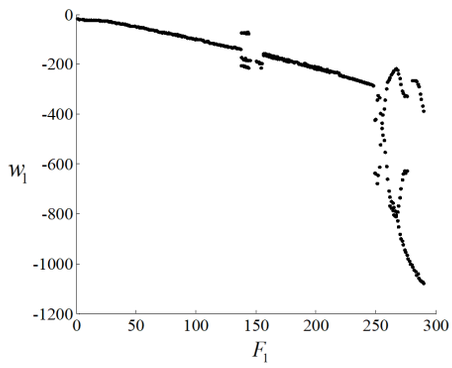

(a)第一阶分叉图

(a)The first-order bifurcation diagram

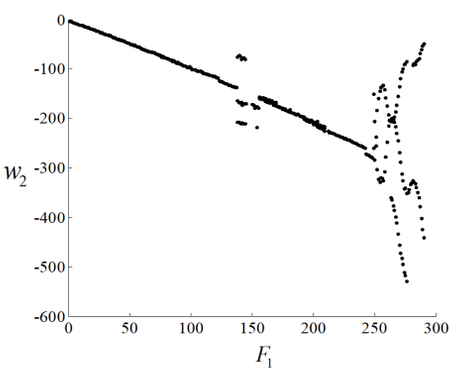

(b)第二阶分叉图

(b)The second-order bifurcation diagram

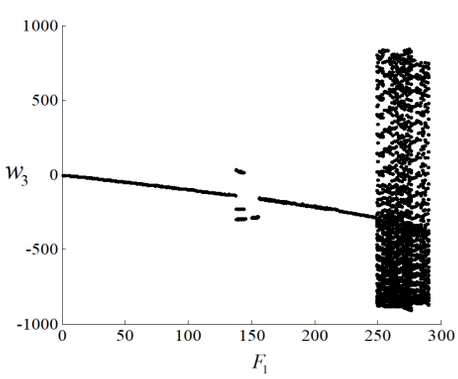

(c)第三阶分叉图

(c)The third-order bifurcation diagram

图 10 系统随三阶外激励变化的分叉图

Fig.10 The bifurcation diagrams of the first three modes with respect to excitation amplitude F_1

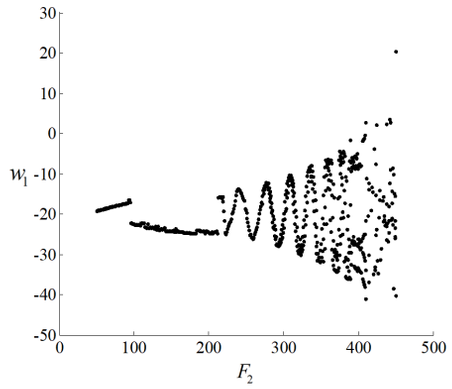

(a)第一阶分叉图

(a)The first-order bifurcation diagram

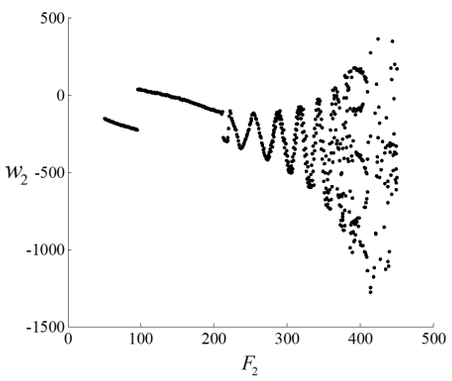

(b)第二阶分叉图

(b)The second-order bifurcation diagram

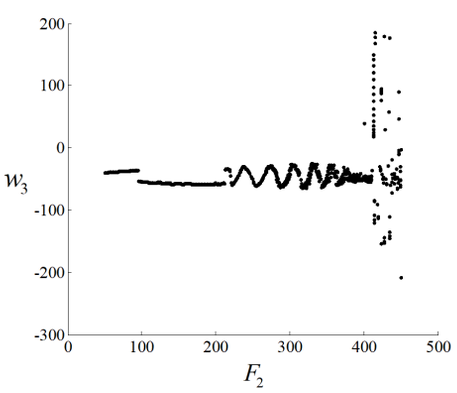

(c)第三阶分叉图

(c)The third-order bifurcation diagram

图 11 系统随三阶外激励变化的分叉图

Fig.11 The bifurcation diagrams of the first three modes with respect to excitation amplitude F_2

由度的无量纲常微分方程.考虑主参数共振-1:3:5共振,分析外激励以及压电系数对系统的非线性响应,然后数值模拟得到不同阶外激励幅值对复合材料悬臂板非线性动力学响应的影响.

数值结果表明,随着长宽比的增加,压电纤维复合材料悬臂板固有频率逐渐降低.在主参数共振-1:3:5内共振关系下,该结构表现出硬弹簧特性,随着外激励以及压电系数的增加,硬弹簧特性更加明显.只改变外激励幅值,不同尺寸的板都会出现周期到混沌的运动,由此可见外激励幅值的改变会对系统的非线性动力学特性产生显著的影响,同时,在不同尺寸下,系统会表现不同的稳定性,随着板尺寸的增加,系统的稳定性降低,板越小,动态

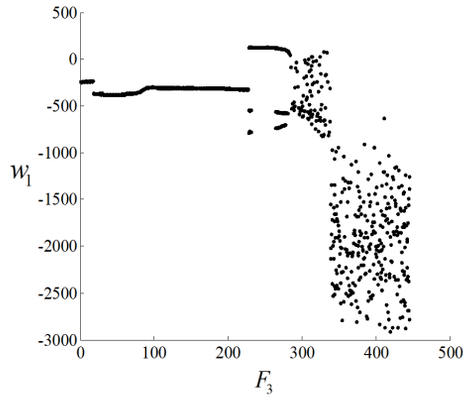

(a)第一阶分叉图

(a)The first-order bifurcation diagram

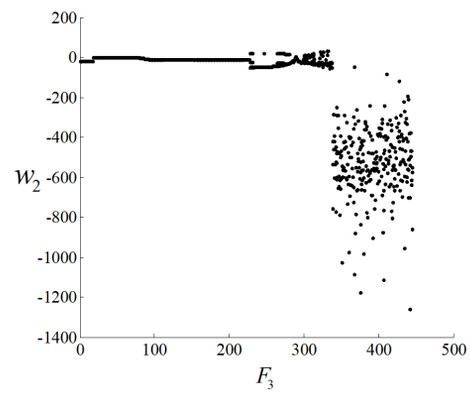

(b)第二阶分叉图

(b)The second-order bifurcation diagram

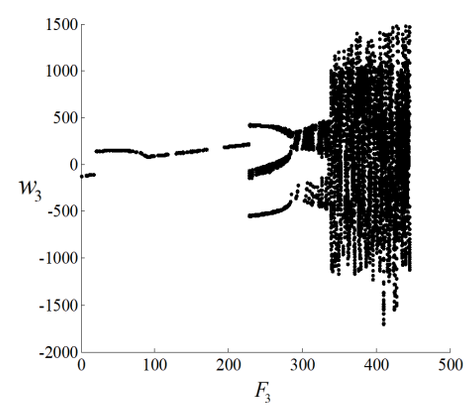

(c)第三阶分叉图

(c)The third-order bifurcation diagram

图 12　系统随三阶外激励变化的分叉图

Fig.12　The bifurcation diagrams of the first three modes with respect to excitation amplitude F_3

稳定区域将越大.通过理论方法研究压电纤维复合板的内部共振和稳定性,对压电纤维复合材料的应用具有重要的理论意义和工程价值.

参　考　文　献

1　Hagood N W, Bent A A. Development of piezoelectric fibber composites for structural actuation. AIAA-1993-1717-CP, 1993

2　Neslon L J. Characterisation and modelling of active fibre composites. Bath: University of Bath, 2005

3　Rossetti G A, Pizzochero J A, Bent A A. Recent advances in active fiber composites technology. IEEE International Symposium on Applications of Ferroelectrics. Honolulu: IEEE, 2000:753~756

4　Shindo Y, Narita F, Sato K, et al. Nonlinear electromechanical fields and localized polarization switching of piezoelectric macro fibber composites. *Journal of Mechanical of Material and Structure*, 2012, 6(7): 1089~1102

5　Prazenica R J, Kim D, Moncayo H, et al. Design characterization and testing of macro-fibber composite actuators for integration on a fixed-wing UAV. In: Proceedings of SPIE-The International Society for Optical Engineering, 2014, 9057(15), 905715

6　Xie C H, Wu Y, Liu Z S. Modeling and active vibration control of lattice grid beam with piezoelectric fiber composite using fractional order PD algorithm. *Composite Structures*, 2018, 198 :126~134

7　Zhang C L, Zhang X N, Xu M L, et al. Active control of honeycomb sandwich plate using MFC piezoelectric actuators. *International Journal of Applied Electromagnetics and Mechanics*, 2014, 45: 83~91

8　Lin X J, Zhou K C, Zhang X Y, et al. Development, modeling and application of piezoelectric fiber composites. *Transactions of Nonferrous Metals Society of China*, 2013, 23(1): 98~107

9　Williams R B, Park G, Inman D J, et al. An overview of composite actuators with piezoceramic fibers. *Proceeding of IMAC XX*, 2002, 47(4): 421~427

10　Xia X K, Shen H S. Nonlinear vibration and dynamic response of FGM plates with piezoelectric fiber reinforced composite actuators. *Composite Structures*, 2009, 90(2): 254~262

11　Shen H S, Zhu Z H. Compressive and thermal postbuckling behaveiors of laminated plates with piezoelectric fiber reinforced composite actutors. *Applied Mathematical Modelling*, 2011, 35, :1829~1845

12　Padoin E, Santos I F, Perondi E A, et al. Topology optimization of piezoelectric macro-fibber composite patches on laminated plates for vibration suppression. *Structure and Multidisciplinary Optimization*, 2018, 59(3): 941~957

13 Guo X Y, Jiang P, Zhang W. Nonlinear dynamic analysis of composite piezoelectric plates with graphene skin. *Composite Structures*, 2018, 206: 839~852

14 Panda S, Ray M C. Active control of geometrically nonlinear vibrations offunctionally graded laminated composite plates using piezoelectric fiberreinforced composites. *Journal of Sound and Vibration*, 2009, 325: 186~205

15 Zhao S G, Cheng W, Guan D. Torsion characteristics of active laminates with 1-3 PFC layers. *Acta Aeronauticaet Astronautica Sinica*, 2006, 27(4): 624~629

16 Xie C H, Wu Y, Liu Z S.A new approach for electro-elastic analysis of piezoelectric fiber composites with arbitrary shaped inclusions under anti-plane shear and in-plane electric loadings. *Smart Materials and Structures*, 2019, 28 (7): 75030

THE INFLUENCE OF DIFFERENT ORDER EXCITATIONS ON RESPONSES OF PIEZOELECTRIC FIBRE COMPOSITE PLATES WITH MULTI INNER RESONANCE *

Guo Xiangying[1,2†] Duan Mengye[1,2]

(1.*Department of Materials and Manufacturing, Beijing University of Technology, Beijing* 100124, *China*)

(2.*Beijing Key Laboratory of Nonlinear Vibrations and Strength of Mechanical Structures, Beijing* 100124, *China*)

Abstract The paper investigates nonlinear dynamical characteristic of a macro fibre composite (MFC) plate subjected to transversal excitations. Nonlinear governing equations for the MFC plate are established based on Reddy's first-order shear deformation theory, von Karman geometrical nonlinear kinematics and Hamilton's principle. To analyze complex inner resonance phenomenon of the MFC plate, the first three order natural frequencies and the relationships of various internal resonances with different physical dimensions are discussed under different order excitations, and Galerkin's approach is employed to discretize the partial differential governing equations into a three-degree-of-freedom nonlinear system. Then, stability analysis is conducted to investigate influences of related parameters on nonlinear behaviors of the composite plate. The results of numerical simulation show that increase of plate size will lead to decrease of both the natural frequencies and dynamic stability of the plate. Moreover, the different order transversal excitation has great effects on the nonlinear dynamics of the structure. The results will provide theoretical supports for practical engineering applications.

Key words MFC, nonlinear dynamics, stability analysis, internal resonance

Received 22 September 2020, revised 22 October 2020.

* The project supported by the National Natural Science Foundation of China (11572006, 11772010)

† Corresponding author E-mail: eagle2008guo@yeah.net